Weak Light H_2O_2 Photosynthesis from H_2O and O_2 by Carbon Nitrides with Piezoelectric Effect for Tumor Therapy

Jin Ma,[a]‡ Cheng Peng,[b]‡, Xiaoxiao Peng,[a] Sicheng Liang,[a] Zhixin Zhou,[a] Kaiqing Wu,[a] Ran Chen,[a] Songqin Liu,[a] Yanfei Shen,[a] Haibo Ma,[b]* Yuanjian Zhang[a]*

[a] Jiangsu Engineering Laboratory of Smart Carbon-Rich Materials and Device, Jiangsu Province Hi-Tech Key Laboratory for Bio-Medical Research, School of Chemistry and Chemical Engineering, Medical School, Southeast University, Nanjing 211189, China, E-mail: Yuanjian.Zhang@seu.edu.cn

[b] Qingdao Institute for Theoretical and Computational Sciences, Qingdao Institute of Frontier and Interdisciplinary Science, Shandong University, Qingdao 266237, China E-mail: haibo.ma@sdu.edu.cn

‡ J. Ma and C. Peng contributed equally to the work.

Abstract

Artificial photocatalysis could be the choice of technology for producing H_2O_2 considering the abundant sunlight exposure in global regions. However, despite recent technological advances, current catalyst systems still remain challenging that the need for high density sunlight, poor selectivity/activity and unfavourable thermodynamics. Here, we reported that carbon nitride with extended conjugation C_5N_2 harness piezoelectric-effect to both change the selectivity/activity of WOR and photogenerated charge kinetics in non-sacrificial H_2O_2 production. Here, C_5N_2 achieves a H_2O_2 photosynthesis rate of 918.4 μM/h and a solar-to-chemical conversion efficiency of 2.6% under a weak sunlight (0.1 sun) and ultrasonic irradiation. Additionally, C_5N_2 exhibited by far the highest piezocatalytic H_2O_2 synthesis activity at rates up to 480.1 μM/h. The new strategy was further applied to efficient SPCDT and water purification in low density light input conditions. This work not only presents piezoelectric-effect of carbon nitride to harness the selectivity/activity of WOR and the migration/transport of photogenerated charges as an available innovative concept in energy, but also sheds light on rising potentials in health and environment.

Introduction

Hydrogen peroxide (H_2O_2), one of the most valuable multifunctional chemicals with strong oxidation power and high energy density[1-5], is widely used in industrial applications, such as clean fuels, wastewater treatment, cleaning, and organic synthesis[6-11]. As an endogenous long-life reactive oxygen species (ROS), H_2O_2 also participate in biological processes and exert versatile physiological and pathological functions, thus has also been extensively used in biomedical sensing, disinfection, and cancer photodynamic therapy (PDT)[12-15]. The primary methods for H_2O_2 synthesis encompass the anthraquinone process, electrocatalytic O_2 reduction, and direct H_2-O_2 reaction[16-20]. However, these methods are challenged by high energy consumption, high cost, and/or serious safety issues. Therefore, an innovative, onsite, green, safe and low-cost H_2O_2 production is imperative desired.

Artificial photocatalysis offers a potential way to drive chemical conversions under very mild conditions[21-25]. Recently, engineering polymeric carbon nitride (pCN)-based photocatalysts has become a promising strategy for overall H_2O_2 production by using water and oxygen as raw materials without any sacrificial agents[26-29]. It involves a $2e^-$ oxygen reduction reaction (ORR, Eq. 1) and a $2e^-$ or $4e^-$ water oxidation reaction (WOR, Eq. 2-5)[30]. Nonetheless, direct $2e^-$ WOR process occurs at higher oxidation potential (+1.76 V vs. NHE, Eq. 3), compared to the $4e^-$ WOR (+1.23 V vs. NHE, Eq. 2). The stepwise $2e^-$ WOR process (Eq. 4-5) requires intermediate hydroxyl radicals (·OH, +2.73 V vs. NHE, Eq. 4), which makes indirect $2e^-$ WOR difficult to occur[31,32]. Therefore, the high uphill thermodynamics of $2e^-$ WOR process significently limit the overall photocatalytic H_2O_2 production, resulting in a low solar-to-chemical conversion (SCC) efficiency[33-36]. In addition, most photocatalysts work under strong light irradiation in laboratory conditions. It makes pratical challenge in photocatlytic H_2O_2 generation in weak light conditions, e.g., under cloudy/overcast circumstances or for deep tissues PDT owing to light scatters[37-40].

2e- ORR:

$$O_2 + 2H^+ + 2e^- \rightarrow H_2O_2 \qquad 0.69 \text{ V vs. NHE} \qquad (1)$$

4e- WOR:

$2H_2O + 4h^+ \rightarrow O_2 + 4H^+$ 1.23 V vs. NHE (2)

Direct 2e- WOR:

$2H_2O + 2h^+ \rightarrow H_2O_2 + 2H^+$ 1.76 V vs. NHE (3)

Indirect 2e- WOR:

$H_2O + h^+ \rightarrow \bullet OH + H^+$ 2.73 V vs. NHE (4)

$2\bullet OH \rightarrow H_2O_2$ 1.14 V vs. NHE (5)

Enhancing the adsorption/activation of water and the formation of *OH intermediate is the key rate-determining step for WOR half-reaction (Fig 1a)[31]. Zare et al. proposed a microdroplet method to prepare H_2O_2, in which an extremely high electric field was formed at the gas-liquid interface of the microdroplet[41,42]. The surface hydroxyl radicals and free electrons were generated at microdroplet interface, which further recombined and generated H_2O_2. Similarily, manipulating piezoelectric effect of noncentral symmetric semiconductors induced by mechanical energy can also change both the selectivity and activity of WOR[43-46]. Piezoelectric effect induced electron hole separation in the polar field can overcome the thermodynamic potential of WOR to directly generate surface active hydroxyl groups that continue to generate hydrogen peroxide[47]. Nonetheless, although these investigations have been carried out at the macroscopic level, the production yield of H_2O_2 was relatively low.

Herein, we proposed a facile approach for the directly enhancement of H_2O_2 photosynthesis efficiency, relying on piezoelectric-effect of carbon nitrides in deionized (DI) water without any sacrificial agents. Under ultrasound treatment, electron exchange could occur between pCN and water with repeated contact and separation cycles at the interface due to the piezoelectric effect. The results shown that the H_2O_2 production rate of C_5N_2 could reached to 918.4 μM/h in weak light (10 mW/cm^2) and 480.1 μM/h in dark without any sacrificial agents and co-catalysts, which exceeds most piezo-photocatalytic processes on carbon nitride and piezo-catalytic processes[45,48-51]. Based on this, C_5N_2 was successfully applied to sono-photo-chemodynamic therapy (SPCDT) for the first time, demonstrating competitive performances. This work would

open a new avenue for highly efficient and selective photosynthesis of H_2O_2, particularly in realistic low density solar conditions, and pave their intriguing applications in energy, health and environments.

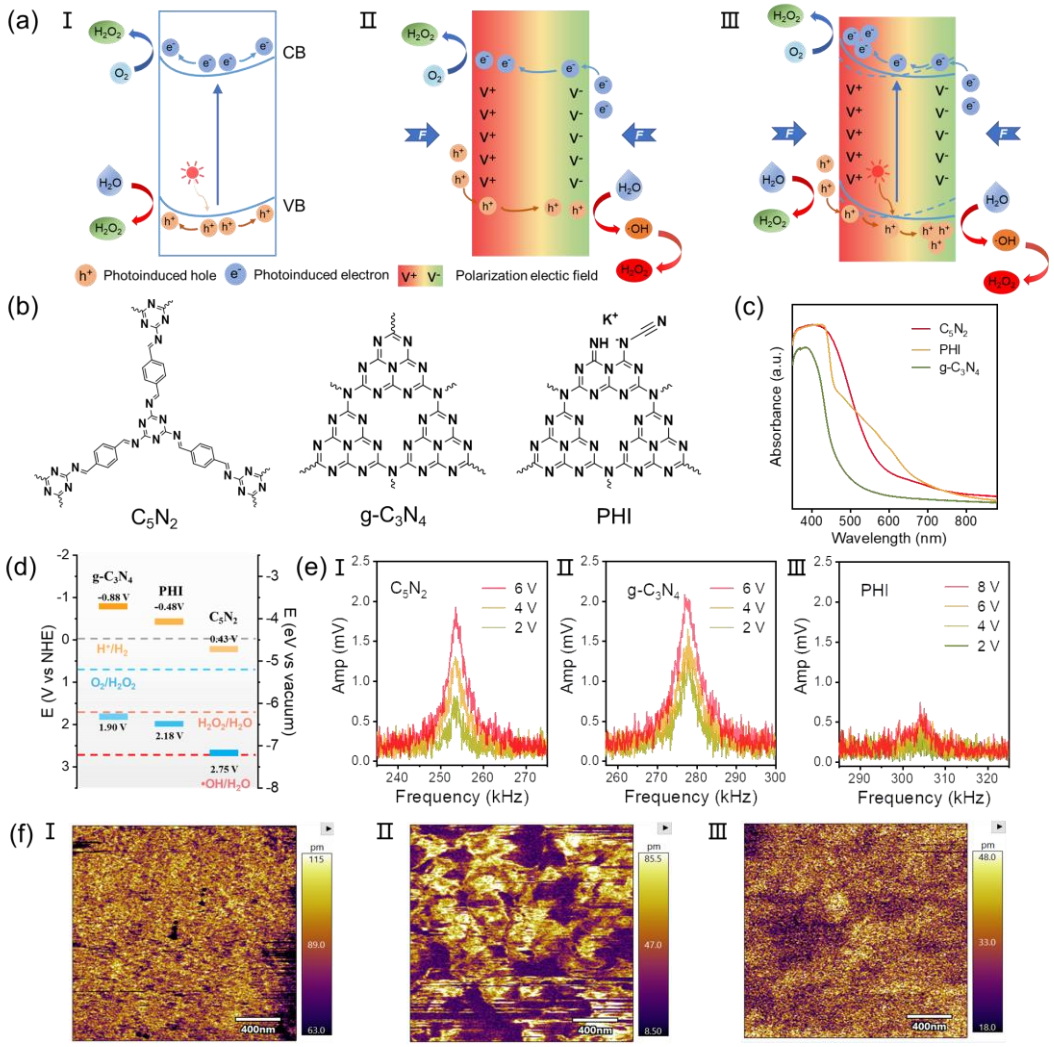

Figure 1. Strategy of a piezoelectric field promoting photocatalytic H_2O_2 overall production. (a) Mechanism of the piezoelectric effect to promote the overall photocatalytic H_2O_2 production. I Photocatalyst without a piezoelectric effect under light irradiation; II Photocatalyst with a piezoelectric effect in the dark and under an external ultrasonic force irradiation; III Photocatalyst with a piezoelectric effect under both light and ultrasonic force irradiation. (b) Molecular structural units of C_5N_2, g-C_3N_4, and PHI. (c) UV-vis DRS of C_5N_2, g-C_3N_4, and PHI. (d) Band positions of g-C_3N_4, PHI and C_5N_2. (e) Resonant peaks for different applied voltages on C_5N_2 g-C_3N_4, and PHI. (f) PFM amplitude images of of (I) C_5N_2, (II) g-C_3N_4 and (III) PHI.

Results and discussion

Materials characterization

C_5N_2 was synthesized via a mild liquid Schiff base reaction, and the control g-C_3N_4 and PHI samples were prepared by a conventional thermal polymerization[13,52]. The molecular structure of pCN-based photocatalysts consist of repetitive triazine or heptazine rings units (Fig.1b). Compared to the idealized g-C_3N_4, C_5N_2 contained a distinct conjugated C=N and benzene linker, and PHI consist of an incomplete heptazine ring with cyanide terminator (C≡N,). The transmission electron microscopy (TEM) images showed g-C_3N_4 and PHI had sheet-like morphologies. The X-ray diffraction (XRD) pattern shown typical two diffraction peaks that can be attributed to the (100) and (002) planes of C_5N_2, g-C_3N_4 and PHI, respectively[53]. The UV-visible absorption spectroscopy was used to explore the optical absorption properties (Fig. 1c). Compared to g-C_3N_4, C_5N_2 and PHI both shown a redshift absorption edge above 460 nm, corresponding to a more narrowed bandgap the g-C_3N_4. It can be explained by the enhanced π-electronic transitions in conjugated CN framework. Likewise, the maximum of photoluminescence wavelength gradually red-shifted, consistent with the narrowed bandgap. As calculated by using UV-Vis spectra and XPS-VB scan spectra[54], a significant downshift of the CB and VB position of C_5N_2 with respect to g-C_3N_4 and PHI was observed, which indicated the order of the water oxidation ability followed as C_5N_2 > PHI > g-C_3N_4 (Fig. 1d).

The anomalous piezoelectric properties of g-C_3N_4, PHI and C_5N_2 were investigated by the piezoresponse force microscopy (PFM). As shown in Figure 1e, three distinct resonant peaks reflecting the piezoelectric vibration excited by voltage in different carbon nitrides were observed. The piezoelectric amplitude of C_5N_2 at the same voltage was comparative to the bulk g-C_3N_4, while that of PHI was weaker. The amplitude exhibits a significant linear correlation with the excitation voltage, confirming the linear piezoelectricity of the pCN-based materials[55]. Moreover, the amplitude signals of all the materials were observed in PFM amplitude mapping (Fig. 1f) and the relaxation of

the piezoelectric domain polarization were also clearly catched through PFM phase analysis[56]. Besides, the PFM amplitude mapping and phase mapping are entirely consistent with the topography, indicating the uniform distribution of polarization in all materials. These results demonstrate that the presence of piezoelectric response in pCN-based materials and could transform pCNs particles into pCNs piezoelectric electrets with sono-catalytic activity during ultrasonic irradiation[57,58].

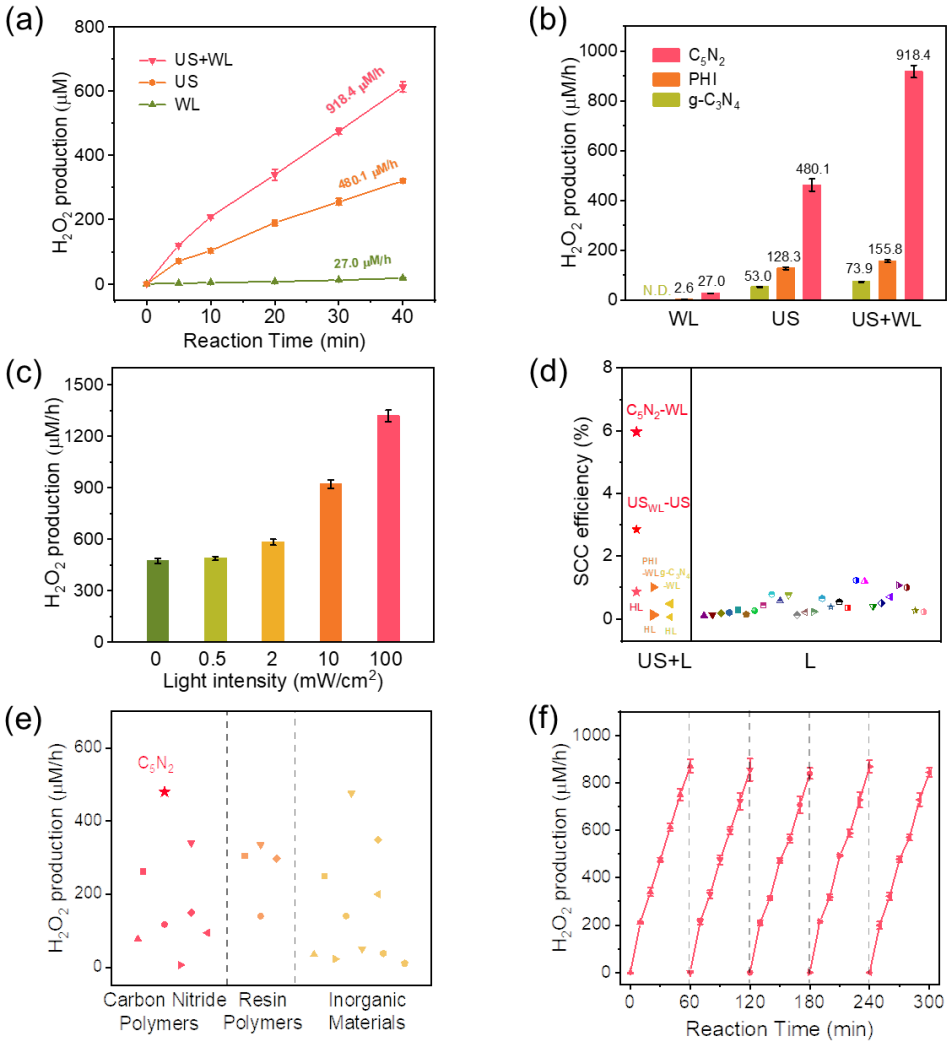

Figure 2. Activity of H_2O_2 piezophotocatalytic production from water and oxygen. (a) Time profiles of H_2O_2 production catalyzed by C_5N_2 in various scenarios. Experimental conditions: 40 mg catalysts in 40 mL of pure water (pH =7) in an ultrasonic cleaner (US, 40 kHz, 400 W) and under weak light (WL, λ> 400 nm, 10 mW cm^{-2}) irradiation, T = 25 °C. (b) Contrastive photosynthetic H_2O_2 activity of g-C_3N_4, PHI and C_5N_2 under WL, US or a combination of them. (c) Comparison of H_2O_2 yields by C_5N_2 under different light intensity in US. (d) Solar-to-chemical

conversion (SCC) efficiency of C_5N_2 (40 mg) in water (40 mL) under WL and US, and summarized SCC efficiencies from reported photocatalysts for H_2O_2 production. (e) Summary Piezoactivity of H_2O_2 production from different reported catalysts under US. (f) Cycling performance for H_2O_2 production under WL and US. Error bars represent the standard deviations of three replicate measurements

Piezoelectric effect in catalytic H_2O_2 production.

To investigate the role of piezoelectric effect in photocatalytic H_2O_2 production, C_5N_2, g-C_3N_4 and PHI were placed in a reactor under both ultrasonic (US) force and visible light (L) conditions. Figure 2a exhibited the H_2O_2 generation rates in 40 minutes achieved on C_5N_2 driven by a weak light (WL) in various scenarios, following the order C_5N_2/US/WL > C_5N_2/US > C_5N_2/ WL. As shown, piezoelectric effect via ultrasonication improved the H_2O_2 production rate of C_5N_2 to 918.4 μM/h in weak light without any sacrificial agents and co-catalysts, which was a nearly 34 times and 2 times enhancement than that under only weak light and ultrasonication driven conditions. The photosynthetic H_2O_2 activity of g-C_3N_4 and PHI were enhanced via the piezoelectric effect (Fig 2b), reaching 73.9 μM/h and 155.8 μM/h, respectively, but far less than that of C_5N_2. Moreover, g-C_3N_4 and PHI can hardly produce H_2O_2 under weak light irradiation. Fig. 2c showed that piezoelectric effect can enhance the photosynthetic H_2O_2 process under different light intensity, and the H_2O_2 production rate of C_5N_2 can reach 1343.6 μM/h without any sacrificial agents in one sun irradiation (100 mW/cm^2). The SCC is the most reliable criterion for photosynthetic H_2O_2 process, which was demonstrated in Fig. 2d. The SCC of C_5N_2 reached 2.6 % in 10% intensity of one sun (10 mW/cm^2), a record in this area[56,59-64]. The as-prepared C_5N_2 not only had advantages in piezophotocatalysis, but also demonstrated by far the highest H_2O_2 piezocatalytic activity (480.1 μM/h) under ultrasonic irradiation among the reported piezocatalysts (Fig 2e) [51,57,65-71]. In addition, the piezophotocatalytic H_2O_2 production rate of C_5N_2 in weak light was well maintained after several repeated cycles, suggesting its excellent stability (Fig 2f).

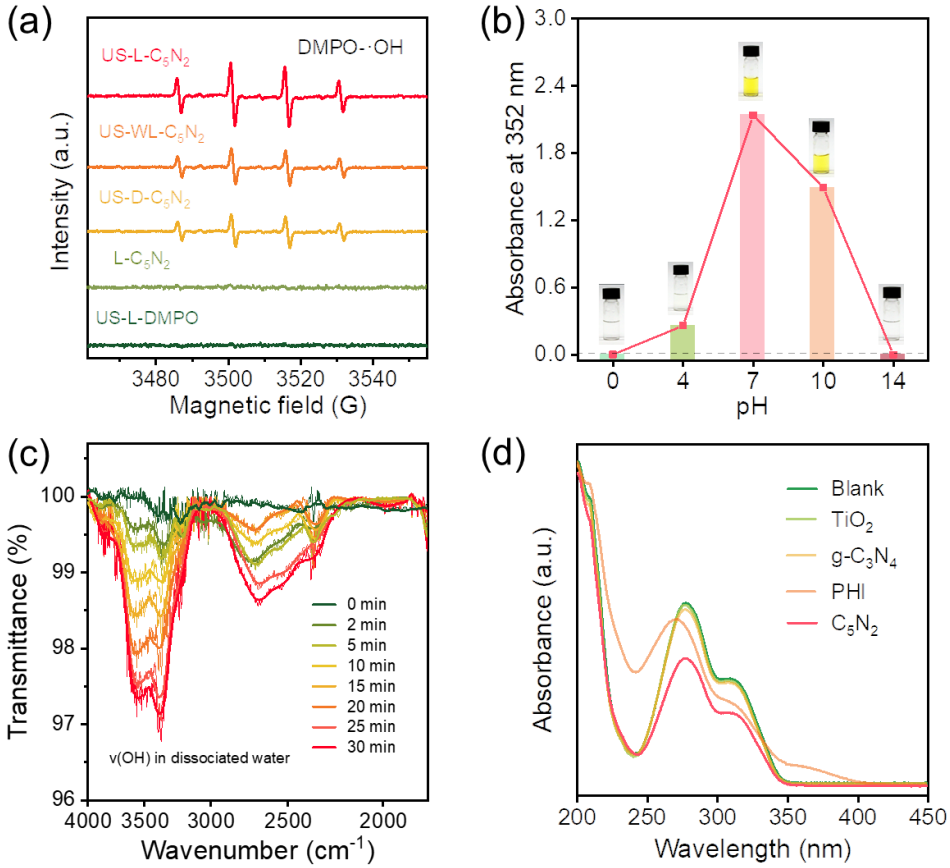

Figure 3. Mechanism of piezophotocatalytic H_2O_2 production. (a) EPR spectra for DMPO-•OH in the presence of C_5N_2 powders under ultrasonication and light irradiation in air atmosphere. (b) Sonophotocatalytic H_2O_2 production by C_5N_2 over a wide pH range (pH 0-14). (c) In situ FTIR spectra of the H_2O dissociation process over C_5N_2 under ultrasonication and light irradiation. (d) UV-Vis absorbance spectra of Cou after reaction with •OH generated by C_5N_2, g-C_3N_4, PHI and TiO_2 before and after ultrasonication and light irradiation.

General charge migration behaviors in photocatalytic H_2O_2 production

Compared with g-C_3N_4 and PHI, the higher performance of C_5N_2 for H_2O_2 production under ultrasonication and weak light suggested the enhanced activity and selectivity of half-reactions during the catalytic process. To identify the mechanisms in H_2O_2 production, WOR and ORR processes were investigated separately to understand insights into the exceptionally high efficiency of piezophotocatalytic H_2O_2 production. For this purpose, the aqueous solutions containing different concentrations of dissolved molecular oxygen were explored. The H_2O_2 production efficiency of C_5N_2 was

relatively higher in the presence of O_2 during the reaction as well as kept nearly half of that in the O_2-saturated one, suggesting an ORR and WOR mode under the C_5N_2/Us/WL system[72]. In this case, when $2e^-$ ORR was inhibited owing to hypoxic conditions, the pathway of WOR would still work for H_2O_2 production. Moreover, the characterization of the intermediates during the photocatalytic H_2O_2 production process via C_5N_2 with ultrasonication (Fig. 3a) were explored to get the formation mechanism for H_2O_2. DMPO and TEMP were used to capture the in situ generated $\bullet O_2^-$, •OH and $^1O_2$, respectively[73,74]. As shown in Figure 3a after ultrasonication and weak light were applied, the $\bullet O_2^-$ and $^1O_2$ signals could not be observed, indicating a direct $2e^-$ ORR process in H_2O_2 production. Moreover, the CB position of C_5N_2 was exceptionally lower than the one-electron ORR potetianal in thermodynamic (-0.33 V vs. NHE), making one-electron reduction of O_2 to form $\bullet O_2^-$ be excluded. In contrast, an increasing significant characteristic quadruplet peak of DMPO-•OH were observed during ultrasonication and weal light irradiation, while negligible signals were observed from the light irradiation-only experiment. In addition, the ability of •OH generation was correlated to the intensity of light irradiation in the C_5N_2/US/WL system.

Next, trapping experiments were performed to examine whether the radicals were produced by electron- hole transfer. It was observed that by adding superoxide, hole, •OH, or electron scavengers, the H_2O_2 production efficiency of C_5N_2 in the C_5N_2/US/WL system demonstrated a various degree of inhibition, indicating not only ORR but also WOR occurred.

In addition, the processes of H_2O_2 production over C_5N_2 for a wide pH range (pH 0–14) were also explored (Fig. 3b). Negligible H_2O_2 was observed from the experimental system with high concentration of H^+ or OH^-, and the optimum pH was at 7. It indicated that both high concentration of H^+ or OH^- would affect the ORR and WOR half-reaction. Isotope experiments were then performed to verify the existence of $2e^-$ WOR in the C_5N_2/Us/WL system[13,75,76]. It was supposed that using $H_2{}^{18}O$, $H_2{}^{18}O_2$ would be produced if $2e^-$ photocatalytic WOR occurred. However, $H_2{}^{18}O_2$ was unstable and demanding to be detected by mass spectroscopy. To circumvent this problem, a well-

known horseradish peroxidase (HRP)-catalyzed oxidation reaction were performed to transfer the ^{18}O atom in $H_2{}^{18}O_2$ into luminol oxide. The liquid chromatography-mass spectra (LC-MS) of the oxidized luminol demonstrated a normal luminol oxide-^{16}O (m/z: 180) peak and a new luminol oxide-^{18}O (m/z: 182 and 184) peaks, while the control in only light irradiation shown a weak luminol oxide-^{18}O (m/z: 182) peak, confirming the enhancement of the $2e^-$ WOR in this C_5N_2/US/L system.

This activity enhancement mechanism on C_5N_2 was further studied by in situ FTIR to analysis of the H_2O dissociation process (Fig. 3c) and by Coumarin oxidation method to quantify the free intermediate via variation absorbance spectra (Fig. 3d)[24,77]. Compared to g-C_3N_4 and PHI, the in situ FTIR spectroscopy of C_5N_2 shows a more increased peak between 3400-3600 cm^{-1} with reaction time. The wavenumber of ~3,630 cm^{-1} was assigned to the stretching vibration of the OH group in water, and a shoulder at a lower wavenumber of ~3,450 $cm^{-1}$was attributed to the production of *OH intermediate from water dissociation. This indicates that *OH is an important intermediate on the surface of C_5N_2.The UV-Vis absorbance variation spectra of Cou shown a similar trend that more cous are consumed in the reaction with C_5N_2 after ultrasonic and light irradiated, indicating that C_5N_2 generates more free hydroxyl radicals.

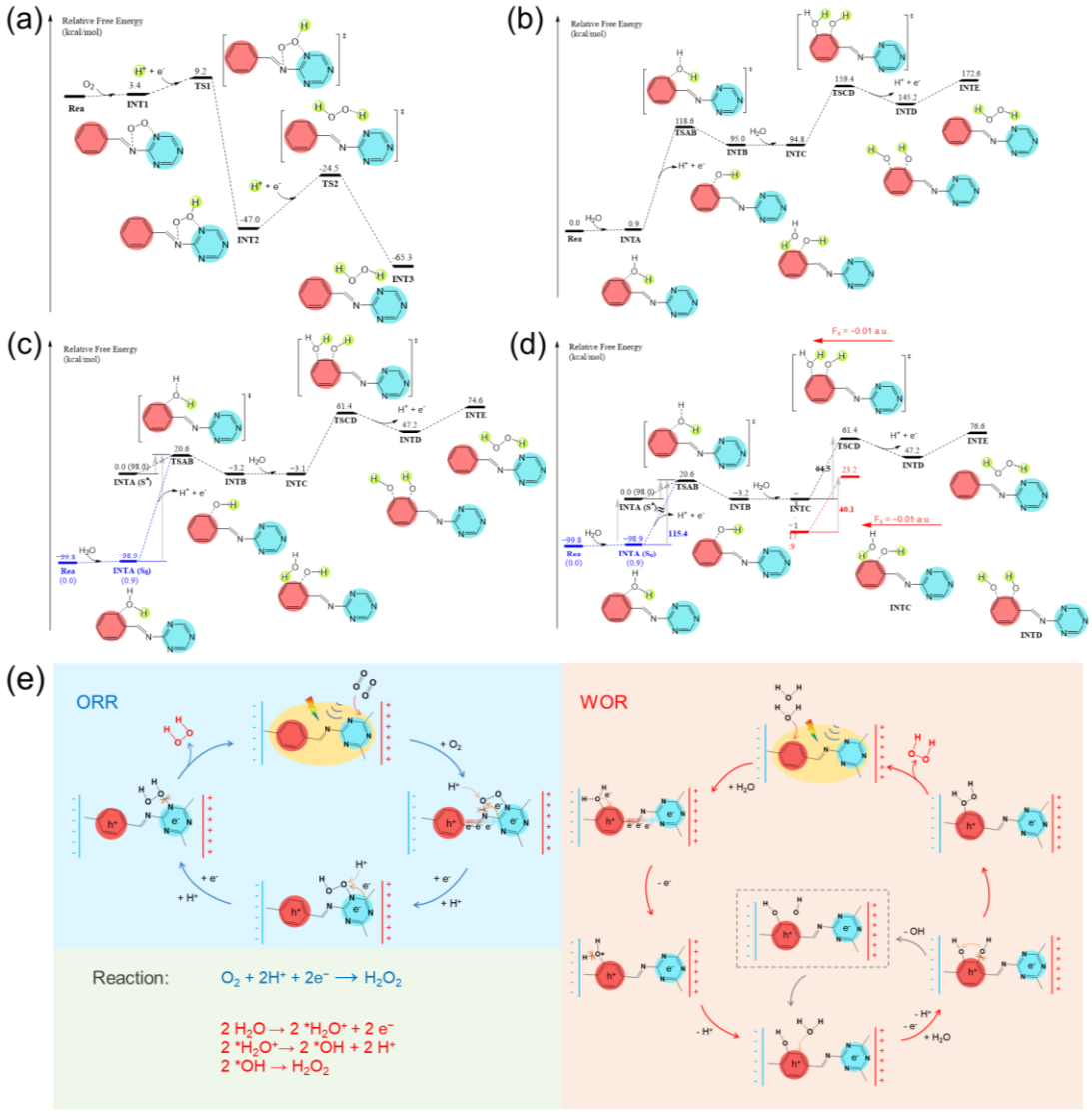

Figure 4. Proposed mechanism of H_2O_2 generation. (a) Free energy profile of the ORR reaction and energies are displayed in kcal/mol at the PCM (H_2O)/B3LYP-D3/6-31G(d,p) level. (b) Free energy profile of the WOR reaction and energies are displayed in kcal/mol at the PCM (H_2O)/B3LYP-D3/6-31G(d,p) level. (c) Free energy profile of the WOR reaction and energies in photocatalysis field are displayed in kcal/mol at the PCM (H_2O)/B3LYP-D3/6-31G(d,p) level. (d) Free energy profile of the WOR reaction and energies in photocatalysis and electric field are displayed in kcal/mol at the PCM (H_2O)/B3LYP-D3/6-31G(d,p) level. The free energy of the photoinduced **INTA** is set as zero and energies (**INTC** and **TSCD**) under electric field (F_x = −0.01 a.u, red arrow) are represented in red. (e) Reaction processes and pathways of ORR and WOR on C_5N_2.

In order to disclose the reaction pathway of the C_5N_2-assisted H_2O_2 generation, density functional theory (DFT) calculation has been carried out and for the sake of simplicity and saving resource, only one building block of the bulk CN is taken into consideration. As shown in Figure 4a (O_2 reduction reaction, ORR), the adsorption configuration of O_2 onto the CN complex surface has been optimized, and the O–N bonding is observed on the NH moieties, which act as the reaction sites in the ORR. For the consequent O_2 reduction, the activated O_2 molecules would combine with protons in the solution to generate *OOH and *HOOH intermediates and finally the product H_2O_2 can be obtained. The transition state involving the formation of H_2O_2 from *OOH is the rate-determining step in the ORR reaction and the calculated free energy barrier (ΔG) of this step is about 22.5 kcal/mol. The process of the water oxidation reaction (WOR) is shown in Figure 4b. H_2O molecules are adsorbed and activated on the benzene ring, and such a transformation would be achieved with a Gibbs activation energy value of about 0.9 kcal/mol. Then H_2O would decompose with generating *OH intermediates. However, the calculated ΔG value for the *OH species formation on the benzene ring through **TSAB** seems thermodynamically unfavorable under the ground state (115.4 kcal/mol). As the reaction is light-induced (Fig. 4c), TD-DFT computational investigation is carried out, in which the result conclusively indicates that the excitation energy of **INTA** is around 98.0 kcal/mol. The activation energy of transition state **TSAB** would decrease to 20.6 kcal/mol, making the following photocatalytic H_2O_2 process possible. Therefore, considering the excitation energy, it is possible for species before **INTA** to serve as kinetically more stable structures with longer lifetime. The photoinduced states are energetically accessible for performing the subsequent bond activation and initiating thereby *OH generation. However, another transition state exhibits a relatively high free energy barrier (64.5 kcal/mol) during the formation of *OH intermediate. Considering the promoting effect of the ultrasonic experimental condition, here the electric field effect is applied to give a qualitative analysis on the reaction mechanism (Fig. 4d). Taking account of the electric fields through calculation, when the electric field intensity increases, the ΔG of *OH generation exhibit a tendency

to decrease, varying from 64.5 kcal/mol (without electric field) to 61.2 and 41.1 kcal/mol (F_x = –0.005 and –0.01 a.u. respectively, Figure S1). Moreover, when the electric field magnitude increases (F_x = –0.012 and –0.0125 a.u.), the reaction mechanism would change, proceeding via a barrierless model. Through theoretical calculation, it can be indicated that the O_2 reduction is thermodynamically more favorable than the water oxidation reaction while both pathways are likely to occur under the experimental conditions. More importantly, the crucial transition state in WOR turns to be more advantageous under applied field, effectively demonstrating the necessity of external ultrasonic environment. These computational findings are not only consistent with the experimental results, but also theoretically prove the high efficiency in the ultrasonic-combined C_5N_2 photocatalytic system. Based on the above experimental and theoretical results, a mechanism of ultrasonic induced WOR to promote photocatalytic synthesis of H_2O_2 over C_5N_2 in the H_2O/O_2 system is proposed (Fig. 4e).

Potential application of Photo/Sono/Chemdynamic Therapy

In conventional cancer therapy, light has been used as a non-invasive therapeutic tool and PDT combined light, photosensitizer(s) and molecular dissolved oxygen (O_2) to generate reactive oxygen species (ROS) that give rise to cellular toxicity[15,78-80]. As another kind of ROS-based therapeutic modality, CDT exploits the endogenous stimulus to in situ generate highly harmful hydroxyl radicals (·OH) from hydrogen peroxide (H_2O_2) through an in-situ Fenton or Fenton-like catalytic reaction[81-83]. As two emerging cancer treatment, PDT and CDT still faces two notable limitations, first, PDT has a lower penetration of light into deep tumor sites as light is required for sensitizer activation; and second, hypoxia and insufficient H_2O_2 cellular environment unable to guarantee sufficient original reagents for ROS synthesis, which seriously limit the therapy efficiency[84,85]. To overcome the drawbacks, many ingenious strategies have been developed, e.g., Improving the light response range of photosensitizers (IR responsed photosensitizers or introducing IR to Vis technology); external transportation

or internal reaction (reactive metal peroxides or water splitting photocatalysts containing photosensitizer, co-catalysts or heterojunction) for improving H_2O_2/O_2 concentration in tumor site; the introduction or combination of external energy fields such as light, ultrasonic, and magnetic field to significantly improve the catalytic reaction kinetics[86-89]. Nonetheless, despite great success in non-sacrificial H_2O_2 production, metal-free polymeric photocatalysts have been rarely explored for SDT/PDT/CDT cancer treatment to enhance the efficiency.

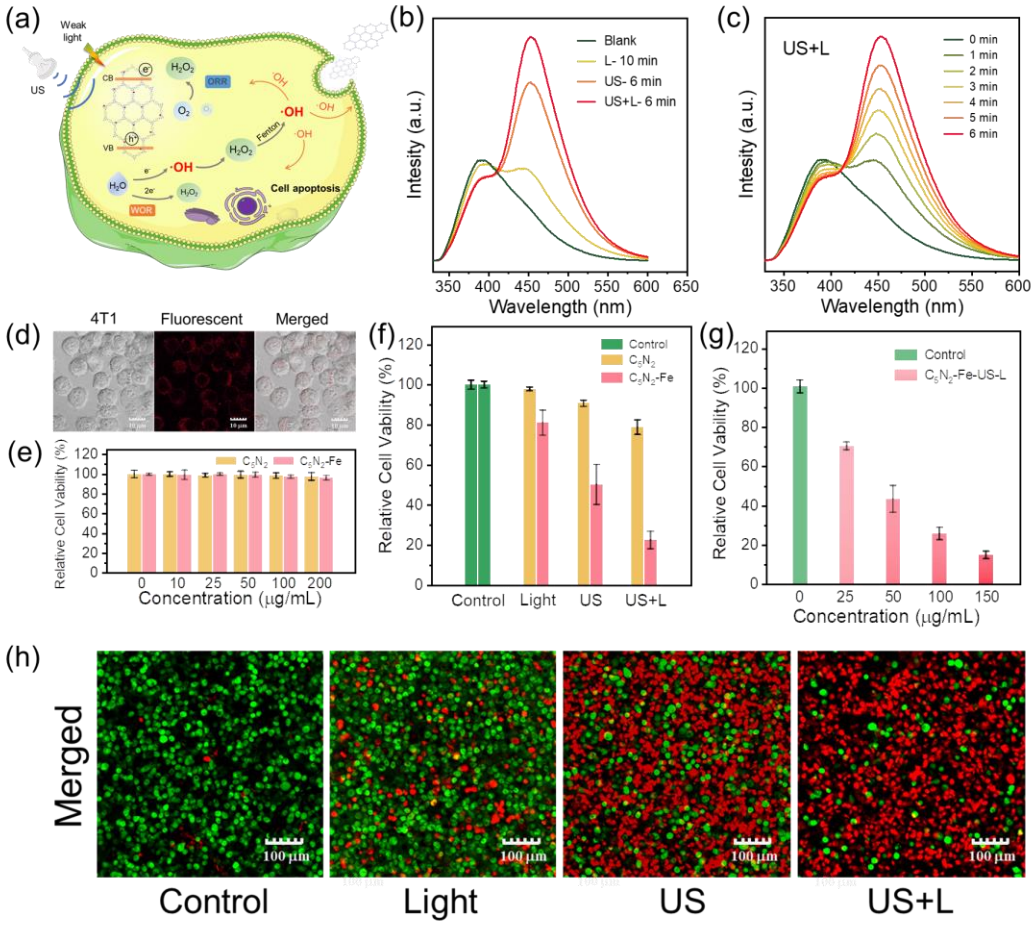

Figure 5. Potential biomedical application of C_5N_2. (a) Scheme of therapeutic processes using C_5N_2 through the Fenton reaction generating •OH under ultrasonic and light irradiation. (b) PL spectra of Cou after reaction with •OH generated by C_5N_2-Fe-NS before and after ultrasonic and light irradiated. (c) PL spectra of Cou after reaction with •OH generated by C_5N_2-Fe-NS before and after ultrasonic and light irradiated. (d). (d) Confocal fluorescence images of 4T1 cells upon incubation with C_5N_2-Fe-NS. (e) Biocompatibility evaluation of C_5N_2-Fe-NS upon incubation with 4T1 cells by WST-8. (f) Cell viability assay by C_5N_2-Fe-NS and C_5N_2-NS treated 4T1 cells in

various scenarios. (g) Cell viability assay by different concentrations of C_5N_2-Fe-NS treated 4T1 cells under ultrasonic and light irradiation. (h) Live/dead double staining of C_5N_2-Fe-NS treated 4T1 cells under ultrasonic and light irradiation indicated by FDA (green, live cells) and PI (red, dead cells).

Controlling intracellular generation of highly toxic hydroxyl radical (•OH) via transition metal ion-mediated Fenton or Fenton-like reaction has been reported as an effective antitumor approach to provide direct potent injury to cancer cell[14,83]. We then developed a C_5N_2-based •OH generator and fluorescence agent for photodynamic and sonodynamic tumor therapy, which exhibited a competitive tumor inhibition effect (Fig. 5a). For this, the pristine C_5N_2 was exfoliated into nanosheets and decorated with Fe ions by a ball milling method (C_5N_2-Fe-NS,)[90,91]. After simple separation, the DLS analysis showed that C_5N_2-Fe-NS displayed a narrow size distribution in aqueous solution, with a hydrodynamic size of ~80 nm; the inset transmission electron microscopy (TEM) image confirmed that C_5N_2-Fe-NS was present as layered nanosheets. Besides, the production of •OH was further demonstrated through the Fenton-like reaction using coumarin (cou) as a probe (Fig. 5b). The probe displayed a new fluorescence emission enhancement at 455 nm upon the reaction to •OH. Compared in light-only, as-produced 7-hydroxy-cou exhibited a gradual amplification of fluorescence intensity with C_5N_2-Fe-NS after adding ultrasonic and light irradiation. Meanwhile, metal ions can react with H_2O_2 generated to produce more •OH, C_5N_2-Fe-NS exhibit the higner fluorescence signal than unmodified C_5N_2-NS. With increased the time of ultrasonic and light irradiation, 7-hydroxy-cou exhibited a gradual amplification of fluorescence intensity, indicating that the ability of the Fenton-like reaction could be sustainably amplified by ultrasonic and light irradiation with C_5N_2-Fe-NS (Fig. 5c)[15,92].

To investigate the accumulation of the C_5N_2-Fe-NS in tumor cells, 4T1 cells were cultured and incubated with C_5N_2-Fe-NS, and the fluorescence confocal imaging was then measured. As shown in Figure 5d, the cytoplasm of the 4T1 cells displayed

prominent fluorescence signals in the red channel, leaving the focal nucleus with no fluorescence. This observation indicated that C_5N_2-Fe-NS was internalized into the cells with specific localization in the cytoplasm. The *in vitro* cytotoxicity of C_5N_2-Fe-NS was accessed in 4T1 cells by 2-(2-Methoxy-4-nitrophenyl)-3-(4-nitrophenyl)-5-(2,4-disulfophenyl)-2H-tetrazolium Sodium Salt (CCK-8) assay. As shown in Fig. 5e, no noticeable adverse effects were observed in cells after 24 h, indicating the excellent biocompatibility of C_5N_2-Fe-NS. To corroborate the critical role of ROS in the therapeutic effect of C_5N_2-Fe-NS, the contribution of SDT/PDT/CDT to total cell death was accessed by carrying out the cell viability under different conditions (Fig. 5f). The cell-killing effect of C_5N_2 or C_5N_2-Fe under US and light irradiation (1.0 MHz, 1.0 W cm^{-2}, 3 min, 50% duty cycle; λ>400nm, 30 mW cm^{-2}, 3min) was significantly increased compared to that of alone treatment of only with US irradiation (1.0 MHz, 1.0 W cm^{-2}, 3 min, 50% duty cycle) or light irradiation (λ>400nm, 30 mW cm^{-2}, 6min), which was mainly attributed to the fact that the C_5N_2-Fe-NS-induced synergistic enhanced effect of SDT, PDT and CDT could produce more significant •OH to induce apoptosis. Meanwhile, compared with the non-Fe involved C_5N_2, C_5N_2-Fe exhibited a significantly increased cell apoptosis and the cell death rate was proportional to the C_5N_2-Fe concentration (Figure 5g), which further evidenced the Fenton-like effect of C_5N_2-Fe for •OH generation to induce cell death. Furthermore, fluorescein diacetate (FDA) and propidium iodide (PI) were utilized to stain the live and dead cells, respectively. Live/dead cell staining assay (Fig. 5h) confirmed a more significant cell death caused by C_5N_2-Fe-NS under both US and light irradiation than only US or light irradiation in cell environments, which were both in accordance with the above cell viability data. These results overall point out that C_5N_2 as a photocatalysts with piezoelectric effect is promising as a highly effective, multifunctional, and safe sono-photosensitizer for enhanced sono-photo-chemodynamic therapy (SPCDT). It's worth mentioning that C_5N_2 not only revealed effective in biomedical therapy systems, but also been allowed its use as novel potential solar-based water purification agents which

are crucial to achieve water disinfection technology in realistic low density sunlight environments.

Conclusion

In summary, we report the polymerization of a triazine and benzyl framework to form extended conjugation C_5N_2, which generates a strong adsorption/activation of water for *OH intermediate groups due to its ideal piezophoto-responsed ability.Compared with traditional carbon nitride (g-C_3N_4 and PHI), the as-prepared C_5N_2 showed an ultrafast photocatalytic H_2O_2 production rate of 918.4 μM/h under weak sunlight and ultrasonic conditions, which surprisingly exhibited a solar-to-chemical conversion efficiency of 2.6% for H_2O_2 synthesis in one-tenth intensity of sun. In addition, C_5N_2 displays a marvelous H_2O_2 yield under only ultrasonic condition, which exceeded most piezosynthetic processes based on carbon nitride or other polymers. Our experimental and theoretical results provide direct evidence for the piezoelectric effect in raising the formation of *OH intermediate groups and speedy generation of H_2O_2 in WOR process. Along this line, a novel C_5N_2 based therapeutic sono-photo-chemodynamic therapy (SPCDT) modality was successfully applied to remove limited light penetration restriction and further induce apparent amplified cancer cell damage in SPCDT with synchronous bioimaging. The potential for piezoelectric effect of the photocatalytic material will be a primary challenge for the continued development of such technology over long-term operation in energy environmental and biomedical fields.

Reference

1 Volokh, M. & Shalom, M. Light on peroxide. *Nat. Catal.* **4**, 350-351 (2021). https://doi.org:10.1038/s41929-021-00620-2

2 Xia, C., Kim, J. Y. & Wang, H. Recommended practice to report selectivity in electrochemical synthesis of H_2O_2. *Nat. Catal.* **3**, 605-607 (2020). https://doi.org:10.1038/s41929-020-0486-1

3 Gong, M. *et al.* Research Progress of Photocatalytic Sterilization over Semiconductors. *RSC. Adv.* **9**, 19278-19284 (2019). https://doi.org:10.1039/c9ra01826c

4 Wang, Q. *et al.* Metal-Free Photocatalysts for Conversion of H_2O into Hydrogen Peroxide. *ChemSusChem* **15** (2022). https://doi.org:10.1002/cssc.202201514

5 Freese, T., Meijer, J. T., Feringa, B. L. & Beil, S. B. An organic perspective on photocatalytic production of hydrogen peroxide. *Nat. Catal.* **6**, 553-558 (2023). https://doi.org:10.1038/s41929-023-00980-x

6 Wang, X. *et al.* Ambient Preparation of Benzoxazine-based Phenolic Resins Enables Long-term Sustainable Photosynthesis of Hydrogen Peroxide. *Angew. Chem. Int. Ed.* **62** (2023). https://doi.org:10.1002/anie.202302829

7 Huang, G.-Z. *et al.* On–Off Switching of a Photocatalytic Overall Reaction through Dynamic Spin-State Transition in a Hofmann Clathrate System. *J. Am. Chem. Soc.* **145**, 26863-26870 (2023). https://doi.org:10.1021/jacs.3c09513

8 Zhang, D. *et al.* Photocatalytic Abstraction of Hydrogen Atoms from Water Using Hydroxylated Graphitic Carbon Nitride for Hydrogenative Coupling Reactions. *Angew. Chem. Int. Ed.* **134** (2022). https://doi.org:10.1002/ange.202204256

9 Chen, J., Ma, Q., Yu, Z., Li, M. & Dong, S. Platinum-Gold Alloy Catalyzes the Aerobic Oxidation of Formic Acid for Hydrogen Peroxide Synthesis. *Angew. Chem. Int. Ed.* **134** (2022). https://doi.org:10.1002/ange.202213930

10 Das, P., Roeser, J. & Thomas, A. Solar Light Driven H_2O_2 Production and Selective Oxidations Using a Covalent Organic Framework Photocatalyst Prepared by a Multicomponent Reaction. *Angew. Chem. Int. Ed.* **62** (2023). https://doi.org:10.1002/anie.202304349

11 Li, Q. *et al.* Shear Stress Triggers Ultrathin-Nanosheet Carbon Nitride Assembly for Photocatalytic H_2O_2 Production Coupled with Selective Alcohol Oxidation. *J. Am. Chem. Soc.* **145**, 20837-20848 (2023). https://doi.org:10.1021/jacs.3c05234

12 Richards, T. *et al.* A residue-free approach to water disinfection using catalytic in situ generation of reactive oxygen species. *Nat. Catal.* **4**, 575-585 (2021). https://doi.org:10.1038/s41929-021-00642-w

13 Ma, J. *et al.* Extended Conjugation Tuning Carbon Nitride for Non-sacrificial H_2O_2 Photosynthesis and Hypoxic Tumor Therapy. *Angew. Chem. Int. Ed.* **61**, e202210856 (2022). https://doi.org:10.1002/anie.202210856

14 Liu, C. *et al.* An Open Source and Reduce Expenditure ROS Generation Strategy for Chemodynamic/Photodynamic Synergistic Therapy. *Nat. Commun.* **11**, 1735 (2020). https://doi.org:10.1038/s41467-020-15591-4

15 Li, P. *et al.* Metal-organic frameworks with photocatalytic bactericidal activity for integrated air cleaning. *Nat. Commun.* **10** (2019). https://doi.org:10.1038/s41467-019-10218-9

16 Yang, S. *et al.* Toward the Decentralized Electrochemical Production of H_2O_2: A Focus on the Catalysis. *ACS Catal.* **8**, 4064-4081 (2018). https://doi.org:10.1021/acscatal.8b00217

17 Yang, H. *et al.* Packing-induced selectivity switching in molecular nanoparticle photocatalysts for hydrogen and hydrogen peroxide production. *Nat. Nanotech.* **18**, 307-315 (2023). https://doi.org:10.1038/s41565-022-01289-9

18 Lu, J. N. *et al.* Synergistic Metal-Nonmetal Active Sites in a Metal-Organic Cage for Efficient Photocatalytic Synthesis of Hydrogen Peroxide in Pure Water.

Angew. Chem. Int. Ed. **62** (2023). https://doi.org:10.1002/anie.202308505

19 Sun, Y., Han, L. & Strasser, P. A comparative perspective of electrochemical and photochemical approaches for catalytic H_2O_2 production. *Chem. Soc. Rev.* **49**, 6605-6631 (2020). https://doi.org:10.1039/d0cs00458h

20 Zhang, Y. *et al.* H_2O_2 generation from O_2 and H_2O on a near-infrared absorbing porphyrin supramolecular photocatalyst. *Nat. Energy* **8**, 361-371 (2023). https://doi.org:10.1038/s41560-023-01218-7

21 Wang, X. *et al.* A Metal-free Polymeric Photocatalyst for Hydrogen Production from Water under Visible Light. *Nat. Mater.* **8**, 76-80 (2009). https://doi.org:10.1038/nmat2317

22 Shiraishi, Y. *et al.* Resorcinol–formaldehyde Resins as Metal-free Semiconductor Photocatalysts for Solar-to-Hydrogen Peroxide Energy Conversion. *Nat. Mater.* **18**, 985-993 (2019). https://doi.org:10.1038/s41563-019-0398-0

23 Hou, H., Zeng, X. & Zhang, X. Production of Hydrogen Peroxide by Photocatalytic Processes. *Angew. Chem. Int. Ed.* **59**, 17356-17376 (2020). https://doi.org:10.1002/anie.201911609

24 Wang, G., Chen, Z., Wang, T., Wang, D. & Mao, J. P and Cu Dual Sites on Graphitic Carbon Nitride for Photocatalytic CO_2 Reduction to Hydrocarbon Fuels with High C_2H_6 Evolution. *Angew. Chem. Int. Ed.* **134** (2022). https://doi.org:10.1002/ange.202210789

25 Schultz, D. M. & Yoon, T. P. Solar Synthesis: Prospects in Visible Light Photocatalysis. *Science* **343** (2014). https://doi.org:10.1126/science.1239176

26 Sun, L. *et al.* A Minireview: The Mechanism of H2O2 Photoproduction by Graphitic Carbon Nitride. *Adv. Energy and Sustain. Research* **4** (2023). https://doi.org:10.1002/aesr.202300090

27 Zhang, Y. *et al.* Molecular Heptazine–Triazine Junction over Carbon Nitride Frameworks for Artificial Photosynthesis of Hydrogen Peroxide. *Adv. Mater.* **35** (2023). https://doi.org:10.1002/adma.202306831

28 Zhang, X. *et al.* Unraveling the Dual Defect Sites in Graphite Carbon Nitride for Ultra-high Photocatalytic H_2O_2 Evolution. *Energy Environ. Sci.* **15**, 830-842 (2022). https://doi.org:10.1039/d1ee02369a

29 Kofuji, Y. *et al.* Carbon Nitride–Aromatic Diimide–Graphene Nanohybrids: Metal-Free Photocatalysts for Solar-to-Hydrogen Peroxide Energy Conversion with 0.2% Efficiency. *J. Am. Chem. Soc.* **138**, 10019-10025 (2016). https://doi.org:10.1021/jacs.6b05806

30 Cheng, H., Cheng, J., Wang, L. & Xu, H. Reaction Pathways toward Sustainable Photosynthesis of Hydrogen Peroxide by Polymer Photocatalysts. *Chem. Mater.* **34**, 4259-4273 (2022). https://doi.org:10.1021/acs.chemmater.2c00936

31 Hu, X. *et al.* Engineering Nonprecious Metal Oxides Electrocatalysts for Two-Electron Water Oxidation to H_2O_2. *Ad. Energy Mater.* **12**, 2201466 (2022). https://doi.org:10.1002/aenm.202201466

32 Chen, D. *et al.* Covalent Organic Frameworks Containing Dual O_2 Reduction Centers for Overall Photosynthetic Hydrogen Peroxide Production. *Angew.*

Chem. Int. Ed. **62** (2023). https://doi.org:10.1002/anie.202217479

33 Ren, P. *et al.* An Atomically Dispersed Mn-Photocatalyst for Generating Hydrogen Peroxide from Seawater via the Water Oxidation Reaction (WOR). *J. Am. Chem. Soc.* **145**, 16584-16596 (2023). https://doi.org:10.1021/jacs.3c03785

34 Tan, H. *et al.* Photocatalysis of Water into Hydrogen Peroxide Over an Atomic Ga-N_5 Site. *Nat. Synth.*, DOI: 10.1038/s44160-44023-00272-z (2023). https://doi.org:10.1038/s44160-023-00272-z

35 Cheng, H. *et al.* Rational Design of Covalent Heptazine Frameworks with Spatially Separated Redox Centers for High-Efficiency Photocatalytic Hydrogen Peroxide Production. *Adv. Mater.* **34**, e2107480 (2022). https://doi.org:10.1002/adma.202107480

36 Yue, J. Y. *et al.* Thiophene-Containing Covalent Organic Frameworks for Overall Photocatalytic H_2O_2 Synthesis in Water and Seawater. *Angew. Chem. Int. Ed.* **62** (2023). https://doi.org:10.1002/anie.202309624

37 Yoon, T. P., Ischay, M. A. & Du, J. Visible light photocatalysis as a greener approach to photochemical synthesis. *Nat. Chem.* **2**, 527-532 (2010). https://doi.org:10.1038/nchem.687

38 Zhang, Y. *et al.* Polyurethane sponge assisted recoverable photocatalyst for outdoor weak sunlight-driven efficient water purification. *Appl. Surface Sci.* **638** (2023). https://doi.org:10.1016/j.apsusc.2023.158091

39 Song, C. *et al.* Atomically dispersed Ni catalyst to boost weak sunlight-driven CO_2 hydrogenation with 100% CO selectivity. *Appl. Surface Sci.* **609** (2023). https://doi.org:10.1016/j.apsusc.2022.155339

40 Harada, N., Sasaki, Y., Hosoyamada, M., Kimizuka, N. & Yanai, N. Discovery of Key TIPS-Naphthalene for Efficient Visible-to-UV Photon Upconversion under Sunlight and Room Light**. *Angew. Chem. Int. Ed.* **133**, 144-149 (2020). https://doi.org:10.1002/ange.202012419

41 Lee, J. K. *et al.* Condensing water vapor to droplets generates hydrogen peroxide. *Proc. Natl. Acad. Sci. USA* **117**, 30934-30941 (2020). https://doi.org:10.1073/pnas.2020158117

42 Chen, B. *et al.* Water–solid contact electrification causes hydrogen peroxide production from hydroxyl radical recombination in sprayed microdroplets. *Proc. Natl. Acad. Sci. USA* **119** (2022). https://doi.org:10.1073/pnas.2209056119

43 Zhou, X., Shen, B., Zhai, J. & Hedin, N. Reactive Oxygenated Species Generated on Iodide-Doped $BiVO_4/BaTiO_3$ Heterostructures with Ag/Cu Nanoparticles by Coupled Piezophototronic Effect and Plasmonic Excitation. *Adv. Funct. Mater.* **31** (2021). https://doi.org:10.1002/adfm.202009594

44 Hu, C. *et al.* Orthogonal Charge Transfer by Precise Positioning of Silver Single Atoms and Clusters on Carbon Nitride for Efficient Piezocatalytic Pure Water Splitting. *Angew. Chem. Int. Ed.* **134** (2022). https://doi.org:10.1002/ange.202212397

45 Zhao, J. *et al.* Contact-electro-catalysis for Direct Synthesis of H_2O_2 under Ambient Conditions. *Angew. Chem. Int. Ed.* **135** (2023).

https://doi.org:10.1002/ange.202300604

46 Pan, L. *et al.* Advances in Piezo-Phototronic Effect Enhanced Photocatalysis and Photoelectrocatalysis. *Adv. Energy Mater.* **10** (2020). https://doi.org:10.1002/aenm.202000214

47 Hu, C. *et al.* Exceptional Cocatalyst-Free Photo-Enhanced Piezocatalytic Hydrogen Evolution of Carbon Nitride Nanosheets from Strong In-Plane Polarization. *Adv. Mater.* **33** (2021). https://doi.org:10.1002/adma.202101751

48 Zhang, X. *et al.* Developing Ni single-atom sites in carbon nitride for efficient photocatalytic H_2O_2 production. *Nat. Commun.* **14** (2023). https://doi.org:10.1038/s41467-023-42887-y

49 Liu, F. *et al.* Covalent organic frameworks for direct photosynthesis of hydrogen peroxide from water, air and sunlight. *Nat. Commun.* **14** (2023). https://doi.org:10.1038/s41467-023-40007-4

50 Fu, M. *et al.* Promoting Piezocatalytic H_2O_2 Production in Pure Water by Loading Metal-Organic Cage-Modified Gold Nanoparticles on Graphitic Carbon Nitride. *Angew. Chem. Int. Ed.*, e202316346 (2023). https://doi.org:10.1002/anie.202316346

51 Wong, K. T. *et al.* Interfacial Schottky Junctions Modulated by Photo-piezoelectric Band Bending to Govern Charge Carrier Migration for Selective H_2O_2 Generation. *Appl. Catal. B Environ.* **315** (2022). https://doi.org:10.1016/j.apcatb.2022.121581

52 Lotsch, B. V. & Schnick, W. From Triazines to Heptazines: Novel Nonmetal Tricyanomelaminates as Precursors for Graphitic Carbon Nitride Materials. *Chem. Mater.* **18**, 1891-1900 (2006). https://doi.org:10.1021/cm052342f

53 Wang, X. *et al.* A Metal-free Polymeric Photocatalyst for Hydrogen Production from Water under Visible Light. *Nat. Mater.* **8**, 76-80 (2008). https://doi.org:10.1038/nmat2317

54 Huang, C. *et al.* Unraveling Fundamental Active Units in Carbon Nitride for Photocatalytic Oxidation Reactions. *Nat. Commun.* **12**, 320 (2021). https://doi.org:10.1038/s41467-020-20521-5

55 Zelisko, M. *et al.* Anomalous Piezoelectricity in Two-dimensional Graphene Nitride Nanosheets. *Nat. Commun.* **5** (2014). https://doi.org:10.1038/ncomms5284

56 Wang, P., Fan, S., Li, X., Duan, J. & Zhang, D. Modulating the Molecular Structure of Graphitic Carbon Nitride for Identifying the Impact of the Piezoelectric Effect on Photocatalytic H_2O_2 Production. *ACS Catal.* **13**, 9515-9523 (2023). https://doi.org:10.1021/acscatal.3c02565

57 Wang, Y. *et al.* Realizing a Strong Visible-light Absorption Band in Piezoelectric 2D Carbon Nitride Sheets for Enhanced Piezocatalysis. *Nano Energy* **104** (2022). https://doi.org:10.1016/j.nanoen.2022.107983

58 Wang, Y. *et al.* Ultrasonic Activation of Inert Poly(tetrafluoroethylene) Enables Piezocatalytic Generation of Reactive Oxygen Species. *Nat. Commun.* **12** (2021). https://doi.org:10.1038/s41467-021-23921-3

59 Tang, R. *et al.* Unique g-C_3N_4/PDI-g-C_3N_4 Homojunction with Synergistic

Piezo-photocatalytic Effect for Aquatic Contaminant Control and H_2O_2 Generation under Visible Light. *Appl. Catal. B Environ.* **303** (2022). https://doi.org:10.1016/j.apcatb.2021.120929

60 Hu, C. *et al.* Exceptional Cocatalyst-Free Photo-Enhanced Piezocatalytic Hydrogen Evolution of Carbon Nitride Nanosheets from Strong In-Plane Polarization. *Adv. Mater.* **33** (2021). https://doi.org:10.1002/adma.202101751

61 Zhou, X. *et al.* Efficient Production of Solar Hydrogen Peroxide Using Piezoelectric Polarization and Photoinduced Charge Transfer of Nanopiezoelectrics Sensitized by Carbon Quantum Dots. *Adv. Sci.* **9** (2022). https://doi.org:10.1002/advs.202105792

62 Zhou, X., Shen, B., Zhai, J. & Hedin, N. Reactive Oxygenated Species Generated on Iodide-Doped $BiVO_4/BaTiO_3$ Heterostructures with Ag/Cu Nanoparticles by Coupled Piezophototronic Effect and Plasmonic Excitation. *Adv. Funct. Mater.* **31** (2021). https://doi.org:10.1002/adfm.202009594

63 Lin, S., Wang, Q., Huang, H. & Zhang, Y. Piezocatalytic and Photocatalytic Hydrogen Peroxide Evolution of Sulfide Solid Solution Nano-Branches from Pure Water and Air. *Small* **18** (2022). https://doi.org:10.1002/smll.202200914

64 Hu, C. *et al.* Coupling Piezocatalysis and Photocatalysis in Bi_4NbO_8X (X=Cl, Br) Polar Single Crystals. *Adv. Funct. Mater.* **30** (2019). https://doi.org:10.1002/adfm.201908168

65 Athanassiadis, A. G. *et al.* Ultrasound-Responsive Systems as Components for Smart Materials. *Chem. Rev.* **122**, 5165-5208 (2021). https://doi.org:10.1021/acs.chemrev.1c00622

66 Wang, Z. L. Piezopotential gated Nanowire Devices: Piezotronics and Piezo-phototronics. *Nano Today* **5**, 540-552 (2010). https://doi.org:10.1016/j.nantod.2010.10.008

67 Fang, L. *et al.* Comparative Investigation of Piezocatalysts Composed of La, Sr and Co (Fe) Complex Oxides in Ruddlesden-Popper Type or Simple Single Perovskites for Efficient Hydrogen Peroxide Generation. *Chem. Eng. J.* **461** (2023). https://doi.org:10.1016/j.cej.2023.141866

68 Ma, Y. *et al.* Bifunctional $RbBiNb_2O_7$/Poly(tetrafluoroethylene) for High-Efficiency Piezocatalytic Hydrogen and Hydrogen Peroxide Production from Pure Water. *Chem. Eng. J.* **446** (2022). https://doi.org:10.1016/j.cej.2022.136958

69 Jia, Y., Wang, K., Li, C. & Liu, S. Efficient Piezocatalytic Hydrogen Peroxide Generation over MAX Phase Piezocatalysts. *Mater Today Sustain* **22** (2023). https://doi.org:10.1016/j.mtsust.2023.100390

70 Xu, T. *et al.* Constructing Crystalline g-C_3N_4/g-$C_3N_{4-x}S_x$ Isotype Heterostructure for Efficient Photocatalytic and Piezocatalytic Performances. *Energy Environ Mater* **6** (2022). https://doi.org:10.1002/eem2.12306

71 Wang, K. *et al.* Enhancing Piezocatalytic H_2O_2 Production through Morphology Control of Graphitic Carbon Nitride. *J Colloid Interface Sci* **648**, 242-250 (2023). https://doi.org:10.1016/j.jcis.2023.05.204

72 Xu, X. *et al.* Conjugated Organic Polymers with Anthraquinone Redox Centers

for Efficient Photocatalytic Hydrogen Peroxide Production from Water and Oxygen under Visible Light Irradiation without Any Additives. *ACS Catal.* **12**, 12954-12963 (2022). https://doi.org:10.1021/acscatal.2c04085

73 Hao, F. *et al.* Photo-Driven Quasi-Topological Transformation Exposing Highly Active Nitrogen Cation Sites for Enhanced Photocatalytic H_2O_2 Production. *Angew. Chem. Int. Ed.* **62** (2023). https://doi.org:10.1002/anie.202315456

74 Peng, X. *et al.* Molecular assembly of carbon nitride-based composite membranes for photocatalytic sterilization and wound healing. *Chem. Sci.* **14**, 4319-4327 (2023). https://doi.org:10.1039/d3sc00642e

75 Wu, K. *et al.* Elucidating Electrocatalytic Oxygen Reduction Kinetics via Intermediates by Time-Dependent Electrochemiluminescence. *Angew. Chem. Int. Ed.* **62** (2023). https://doi.org:10.1002/anie.202217078

76 Peng, Y. *et al.* Room-Temperature Synthesized Iron/Cobalt Metal–Organic Framework Nanosheets with Highly Efficient Catalytic Activity toward Luminol Chemiluminescence Reaction. *Anal. Chem.* **95**, 18436-18442 (2023). https://doi.org:10.1021/acs.analchem.3c03538

77 Hong, Q. *et al.* Adaptable Graphitic C_6N_6-based Copper Single-atom Catalyst for Intelligent Biosensing. *Nat. Commun.* **14** (2023). https://doi.org:10.1038/s41467-023-38459-9

78 Chen, W. *et al.* A C_5N_2 Nanoparticle Based Direct Nucleus Delivery Platform for Synergistic Cancer Therapy. *Angew. Chem. Int. Ed.* **131**, 6356-6360 (2019). https://doi.org:10.1002/ange.201900884

79 Dewaele, M., Maes, H. & Agostinis, P. ROS-Mediated Mechanisms of Autophagy Stimulation and their Relevance in Cancer Therapy. *Autophagy* **6**, 838-854 (2014). https://doi.org:10.4161/auto.6.7.12113

80 Yang, B., Chen, Y. & Shi, J. Reactive Oxygen Species (ROS)-Based Nanomedicine. *Chem. Rev.* **119**, 4881-4985 (2019). https://doi.org:10.1021/acs.chemrev.8b00626

81 Li, S. L., Jiang, P., Jiang, F. L. & Liu, Y. Recent Advances in Nanomaterial-Based Nanoplatforms for Chemodynamic Cancer Therapy. *Adv. Funct. Mater.* **31**, e2100243 (2021). https://doi.org:ARTN 2100243
10.1002/adfm.202100243

82 Cao, C., Wang, X., Yang, N., Song, X. & Dong, X. Recent Advances of Cancer Chemodynamic Therapy based on Fenton/Fenton-like Chemistry. *Chem Sci.* **13**, 863-889 (2022). https://doi.org:10.1039/d1sc05482a

83 Jia, C., Guo, Y. & Wu, F. G. Chemodynamic Therapy via Fenton and Fenton-Like Nanomaterials: Strategies and Recent Advances. *Small* **18**, e2103868 (2021). https://doi.org:10.1002/smll.202103868

84 Zhao, X., Liu, J., Fan, J., Chao, H. & Peng, X. Recent Progress in Photosensitizers for Overcoming the Challenges of Photodynamic Therapy: from Molecular Design to Application. *Chem. Soc. Rev.* **50**, 4185-4219 (2021). https://doi.org:10.1039/d0cs00173b

85 Liu, J.-n., Bu, W. & Shi, J. Chemical Design and Synthesis of Functionalized Probes for Imaging and Treating Tumor Hypoxia. *Chem. Rev.* **117**, 6160-6224

(2017). https://doi.org:10.1021/acs.chemrev.6b00525

86 Deng, L. *et al.* Low-intensity focused ultrasound-augmented Cascade chemodynamic therapy via boosting ROS generation. *Biomaterials* **271** (2021). https://doi.org:10.1016/j.biomaterials.2021.120710

87 Jana, D. *et al.* Hybrid Carbon Dot Assembly as a Reactive Oxygen Species Nanogenerator for Ultrasound-Assisted Tumor Ablation. *JACS Au* **1**, 2328-2338 (2021). https://doi.org:10.1021/jacsau.1c00422

88 Liang, S., Deng, X., Ma, P. a., Cheng, Z. & Lin, J. Recent Advances in Nanomaterial-Assisted Combinational Sonodynamic Cancer Therapy. *Adv. Mater.* **32** (2020). https://doi.org:10.1002/adma.202003214

89 Gong, F. *et al.* Preparation of TiH1.924 nanodots by liquid-phase exfoliation for enhanced sonodynamic cancer therapy. *Nat. Commun.* **11** (2020). https://doi.org:10.1038/s41467-020-17485-x

90 Han, G.-F. *et al.* Mechanochemistry for ammonia synthesis under mild conditions. *Nat. Nanotech.* **16**, 325-330 (2020). https://doi.org:10.1038/s41565-020-00809-9

91 Ji, J. *et al.* Simultaneous Noncovalent Modification and Exfoliation of 2D Carbon Nitride for Enhanced Electrochemiluminescent Biosensing. *J. Am. Chem. Soc.* **139**, 11698-11701 (2017). https://doi.org:10.1021/jacs.7b06708

92 Cao, X. *et al.* Insight into Iron Leaching from an Ascorbate-Oxidase-like Fe−N−C Nanozyme and Oxygen Reduction Selectivity**. *Angew. Chem. Int. Ed.* **62** (2023). https://doi.org:10.1002/anie.202302463